AAS 03-604

IMPLICIT SPACECRAFT GYRO CALIBRATION

Richard R. Harman[†] **Itzhack Y. Bar-Itzhack**[*]

This paper presents an implicit algorithm for spacecraft onboard instrument calibration, particularly to onboard gyro calibration. This work is an extension of previous work that was done where an explicit gyro calibration algorithm was applied to the AQUA spacecraft gyros. The algorithm presented in this paper was tested using simulated data and real data that were downloaded from the Microwave Anisotropy Probe (MAP) spacecraft. The calibration tests gave very good results. A comparison between the use of the implicit calibration algorithm used here with the explicit algorithm used for AQUA spacecraft indicates that both provide an excellent estimation of the gyro calibration parameters with similar accuracies.

[†] Aerospace Engineer, Tel: 301-286-5125, Fax: 301-286-0369
Flight Dynamics Analysis Branch, Code 595
Mission Engineering and Systems Analysis Division
NASA-Goddard Space Flight Center
Greenbelt, MD 20771
Email: richard.r.harman@nasa.gov

[*] Sophie and William Shamban Professor of Aerospace Engineering
Technion-Israel Institute of Technology. Asher Space Research Institute
Haifa 32000, Israel. Tel: 972-4-829-3196, Fax: 972-4-823-1948
Email: ibaritz@technion.ac.il

I. INTRODUCTION

Previous high fidelity onboard attitude algorithms estimated only the spacecraft attitude and gyro bias. The desire to promote spacecraft and ground autonomy and improvements in onboard computing power has spurred development of more sophisticated calibration algorithms. Namely, there is a desire to provide for sensor calibration through calibration parameter estimation onboard the spacecraft as well as autonomous estimation on the ground.

Gyro calibration is a particularly challenging area of research. There are a variety of gyro devices available for any prospective mission ranging from inexpensive, low fidelity gyros with potentially unstable scale factors, to much more expensive, extremely stable high fidelity units.

Calibration involves two steps. In the first step the instrument error parameters are estimated. During the second step those errors are continuously removed from the gyro readings. There are two approaches to the problem of estimating gyro error parameters. The approach used in the past at the NASA Goddard Flight Dynamics Analysis Branch treated the gyro outputs as angular rate measurements, which are compared to an estimated angular rate. However, this approach requires the knowledge of the angular rate. In the past[1] the estimated angular rate was computed in a rather simplistic way assuming that the rate was constant. To avoid this restriction an algorithm was developed[2] where the estimated angular rate was derived using a Kalman filter (KF) whose input could be any kind of attitude measurement. Therefore the angular rate experienced by the SC could be continuously changing and yet a good estimate of the

rate, necessary for calibration, could be obtained. This approach was named the *explicit approach*. It is described in Fig. 1. Actually, the tasks of the Rate Estimator and the Calibration-Parameter Estimator were done by a single augmented-state KF algorithm.

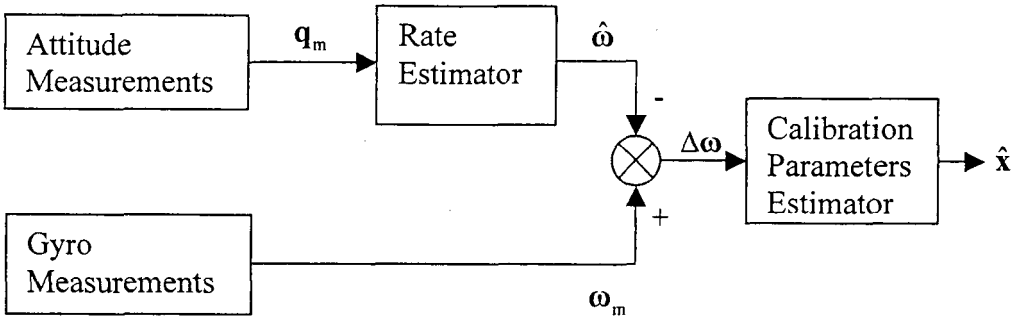

Fig. 1: Explicit Estimation of the Calibration Parameters.

In the classical approach to gyro calibration the gyro outputs are used to maintain or compute body orientation rather than being used as measurements in the context of filtering. In inertial navigation, for example[3], gyro errors cause erroneous computation of velocity and position; then when the latter are compared to measured velocity and position, a great portion of the computed velocity and position errors can be determined. The latter errors are then fed into a Kalman filter (KF) that uses the INS error model to infer the gyro errors. Similarly, when applying the classical approach to spacecraft (SC) attitude determination, the gyro outputs are used to propagate the attitude. Attitude measurements are then used to determine the attitude errors, coupled with a KF, provides an indication of the gyro errors. This approach, which we name the *implicit approach*, is described in block diagrams in Fig. 2. Similar to the *explicit approach*, here too the Attitude Estimation function and the Calibration-Parameter Estimation are performed by a single augmented-state KF algorithm.

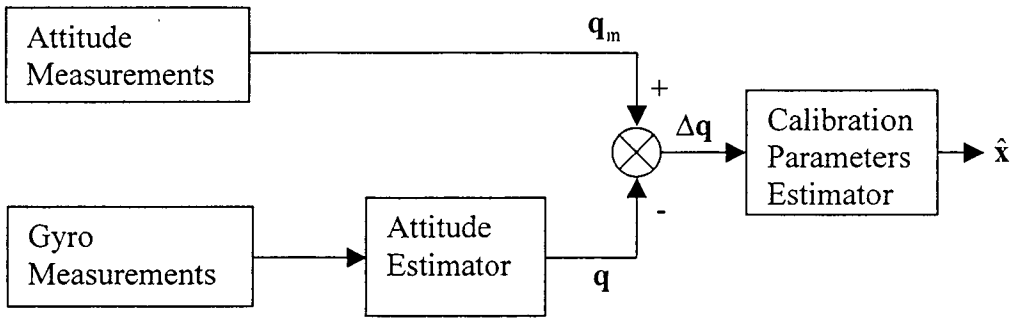

Fig. 2: Implicit Estimation of the Calibration Parameters.

The *explicit approach* is the approach used at NASA Goddard and an extension of it was presented in Ref. 2. The work reported in the present paper is a follow up on the calibration method presented in Ref. 2. The calibration algorithm presented in this work, though, is an *implicit* calibration algorithm, derived here for a standard gyro triad whose sensitive axes are aligned with the SC body axes rather than the AQUA spacecraft case of Ref. 2. The main purpose of the present work is to compare the results obtained using the *explicit approach* with that obtained when using the present *implicit approach.*

In the present work the *implicit approach* was applied to the gyro package of the Microwave Anisotropy Probe (MAP) satellite. The latter consists of two two-axis gyros, which are given the task of measuring the three components (with one redundant axis) of the SC angular velocity vector resolved in the body Cartesian coordinates.

In the next section the gyro error model is derived. Section III presents the implicit approach algorithm for computing the calibration parameters. Section IV presents the compensation procedure that needs to take place to complete the calibration process. In section V the simulation and flight results are presented, and finally in Section VI, the conclusions are presented.

II. GYRO ERROR MODEL

The gyro errors that are considered in this work are: misalignment, scale factor error, and bias (constant drift rate). The gyro error model is a linear model, which associates small error sources to the gyro outputs. *Due to the linearity of the model we can compute the contribution of each error source independently and then sum up all the contributions into one linear model.* We start the description of the error model, by deriving the expression for the gyro misalignments.

II.1 Misalignment Model

The assumed direction of the sensitive axis of gyro *x*, which is one of the three gyro axes, is presented in Fig. 3. The body coordinate axes are also presented and are denoted by **X**, **Y**, and **Z**. The orientation of this gyro is expressed by a vector of unit length in the

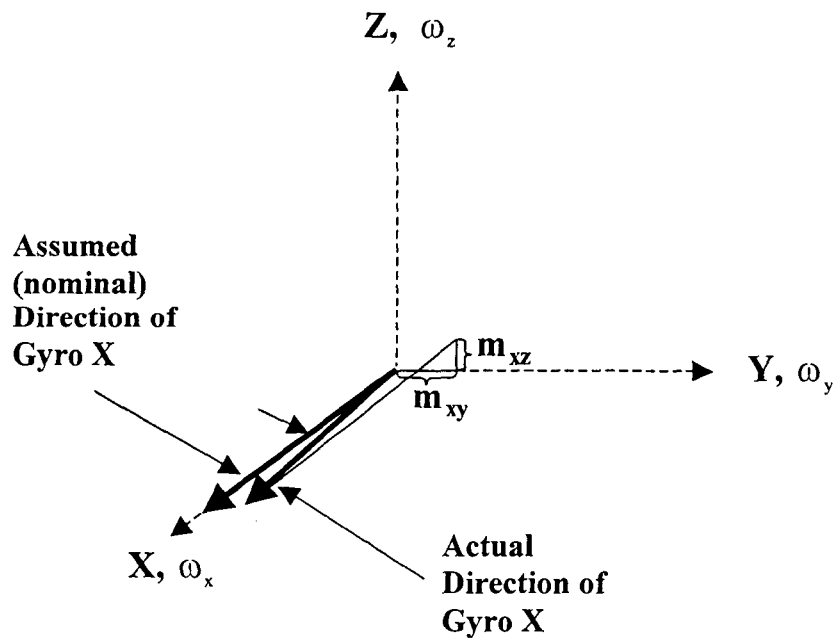

Fig. 3: Misalignment definition of the *x*-gyro sensitive axis.

direction of the gyro sensitive axis. The resulting rate error due to misalignment of all three gyros is:

$$\Delta\boldsymbol{\omega}^m = \begin{bmatrix} \omega_y & \omega_z & 0 & 0 & 0 & 0 \\ 0 & 0 & \omega_x & \omega_z & 0 & 0 \\ 0 & 0 & 0 & 0 & \omega_x & \omega_y \end{bmatrix} \begin{bmatrix} m_{xy} \\ m_{xz} \\ m_{yx} \\ m_{yz} \\ m_{zx} \\ m_{zy} \end{bmatrix} \tag{1}$$

where m_{ij} are the misalignment angles, assumed to be small and $\omega_{x,y,z}$ are the angular velocity components measured by the gyros.

Let,

$$\Omega^m = \begin{bmatrix} \omega_y & \omega_z & 0 & 0 & 0 & 0 \\ 0 & 0 & \omega_x & \omega_z & 0 & 0 \\ 0 & 0 & 0 & 0 & \omega_x & \omega_y \end{bmatrix} \tag{2}$$

and

$$\mathbf{m} = \begin{bmatrix} m_{xy} \\ m_{xz} \\ m_{yx} \\ m_{yz} \\ m_{zx} \\ m_{zy} \end{bmatrix} \tag{3}$$

Then Eq. (1) can be rewritten as,

$$\Delta\boldsymbol{\omega}^m = \Omega^m \mathbf{m} \tag{4}$$

II.2 Scale Factor Error Model

As mentioned, another error source that causes the difference between the correct value of the actual rates and their measurements are the scale factor errors. The error model for the scale factor error is simply

$$\Delta\boldsymbol{\omega}^k = \begin{bmatrix} \omega_x k_x \\ \omega_y k_y \\ \omega_z k_z \end{bmatrix} \tag{5}$$

where the superscript *k* denotes that this error is caused by gyro scale factor errors, and k_i is the scale factor error of gyro i, i = x, y, z. Eq. (5) can be written as follows

$$\Delta\boldsymbol{\omega}^k = \begin{bmatrix} \omega_x & 0 & 0 \\ 0 & \omega_y & 0 \\ 0 & 0 & \omega_z \end{bmatrix} \begin{bmatrix} k_x \\ k_y \\ k_z \end{bmatrix} \tag{6}$$

Define

$$\Omega^k = \begin{bmatrix} \omega_x & 0 & 0 \\ 0 & \omega_y & 0 \\ 0 & 0 & \omega_z \end{bmatrix} \tag{7.a}$$

and

$$\mathbf{k}^T = \begin{bmatrix} k_x & k_y & k_z \end{bmatrix} \tag{7.b}$$

then Eq. (6) can be written as

$$\Delta\boldsymbol{\omega}^k = \Omega^k \mathbf{k} \tag{7.c}$$

II.3 Bias Model

The bias error model is quite simple and is given by

$$\Delta\omega^b = I_3 \mathbf{b} \tag{8}$$

where

$$\mathbf{b} = \begin{bmatrix} b_x \\ b_y \\ b_z \end{bmatrix}$$

and x, y, z are the corresponding gyro axes.

II.4 The Augmented Gyro Error Model

The total gyro error is the sum of all the error discussed before; namely, misalignment, scale factor and bias errors; that is

$$\Delta\boldsymbol{\omega} = \Delta\boldsymbol{\omega}^{m} + \Delta\boldsymbol{\omega}^{k} + \Delta\boldsymbol{\omega}^{b} \tag{9.a}$$

or using Eqs. (4), (7.c), and (8)

$$\Delta\boldsymbol{\omega} = \Omega^{m}\mathbf{m} + \Omega^{k}\mathbf{k} + I_3\mathbf{b} \tag{9.b}$$

The last equation can be written in the following form

$$\Delta\boldsymbol{\omega} = \begin{bmatrix} \Omega^{m} & \Omega^{k} & I_3 \end{bmatrix} \begin{bmatrix} \mathbf{m} \\ \mathbf{k} \\ \mathbf{b} \end{bmatrix} \tag{9.c}$$

Define $H(\boldsymbol{\omega})$ as follows

$$H(\boldsymbol{\omega}) = \begin{bmatrix} \Omega^{m} & \Omega^{k} & I_3 \end{bmatrix} \tag{9.d}$$

also let

$$\mathbf{x} = \begin{bmatrix} \mathbf{m} \\ \mathbf{k} \\ \mathbf{b} \end{bmatrix} \tag{9.e}$$

then Eq. (9.c) can be written as

$$\Delta\boldsymbol{\omega} = H(\boldsymbol{\omega})\mathbf{x} \tag{9.f}$$

III. CALIBRATION-PARAMETERS ESTIMATION

III.a The Dynamics Model

Our goal now is to estimate $\mathbf{x}$, and for that we need to know how $\mathbf{x}$ influences the attitude estimation. The true quaternion solves the differential equation

$$\dot{\mathbf{q}} = \frac{1}{2}\Omega\mathbf{q} \tag{10.a}$$

where

$$\Omega = \begin{bmatrix} 0 & \omega_z & -\omega_y & \omega_x \\ -\omega_z & 0 & \omega_x & \omega_y \\ \omega_y & -\omega_x & 0 & \omega_z \\ -\omega_x & -\omega_y & -\omega_z & 0 \end{bmatrix} \tag{10.b}$$

The measured angular rate, $\boldsymbol{\omega}_m$, contains the gyro error, $\Delta\boldsymbol{\omega}$, thus

$$\boldsymbol{\omega}_m = \boldsymbol{\omega} + \Delta\boldsymbol{\omega} \tag{10.c}$$

consequently

$$\Omega = \Omega_m - \delta\Omega \tag{10.d}$$

where Ω_m as well as $\delta\Omega$ are in the format of Eq. (10.b). Using the last equation, Eq. (10.a) can be written as:

$$\dot{\mathbf{q}} = \frac{1}{2}\Omega_m\mathbf{q} - \frac{1}{2}\delta\Omega\mathbf{q} \tag{10.e}$$

which can be written as

$$\dot{\mathbf{q}} = \frac{1}{2}\Omega_m\mathbf{q} - \frac{1}{2}Q\cdot\Delta\boldsymbol{\omega} \tag{10.f}$$

where

$$\Omega_m = \begin{bmatrix} 0 & \omega_{z,m} & -\omega_{y,m} & \omega_{x,m} \\ -\omega_{z,m} & 0 & \omega_{x,m} & \omega_{y,m} \\ \omega_{y,m} & -\omega_{x,m} & 0 & \omega_{z,m} \\ -\omega_{x,m} & -\omega_{y,m} & -\omega_{z,m} & 0 \end{bmatrix} \tag{10.g}$$

and Q is given by

$$Q = \begin{bmatrix} q_4 & -q_3 & q_2 \\ q_3 & q_4 & -q_1 \\ -q_2 & q_1 & q_4 \\ -q_1 & -q_2 & -q_3 \end{bmatrix} \tag{10.h}$$

Using Eq. (9.f) in Eq. (10.f) yields

$$\dot{\mathbf{q}} = \frac{1}{2}\Omega_m \mathbf{q} - \frac{1}{2} QH(\boldsymbol{\omega})\mathbf{x} \tag{10.i}$$

Since we do not know $\boldsymbol{\omega}$, as a common practice, we use instead the measured angular rate, $\boldsymbol{\omega}_m$. Equation (10.i) becomes

$$\dot{\mathbf{q}} = \frac{1}{2}\Omega_m \mathbf{q} - \frac{1}{2} QH(\boldsymbol{\omega}_m)\mathbf{x} \tag{11.a}$$

Because $\mathbf{x}$ is a constant vector we can write

$$\dot{\mathbf{x}} = 0 \tag{11.b}$$

Augmenting the last two equations yields

$$\begin{bmatrix} \dot{\mathbf{q}} \\ \dot{\mathbf{x}} \end{bmatrix} = \begin{bmatrix} \frac{1}{2}\Omega_m & -\frac{1}{2} QH(\boldsymbol{\omega}_m) \\ 0 & 0 \end{bmatrix} \begin{bmatrix} \mathbf{q} \\ \mathbf{x} \end{bmatrix} + \begin{bmatrix} \mathbf{w}_q \\ \mathbf{w}_x \end{bmatrix} \tag{11.c}$$

where ω_q and ω_x are dynamics noise terms. Initially the matrix Q is evaluated using $\mathbf{q}_m$. When the attitude converges it is better to use $\hat{\mathbf{q}}$, the estimated quaternion. Similarly, initially we use $\boldsymbol{\omega}_m$ to evaluate H. As the estimate of $\mathbf{x}$ converges, we compensate the gyro readings (as shown in the next section), then compensated gyro readings are closer to $\boldsymbol{\omega}$. Therefore we can use the compensated angular rate, $\hat{\boldsymbol{\omega}}$, in H of Eq. (11.c).

III.b Measurement Model

For quaternions the measurement model becomes:

$$\mathbf{q}_m = \begin{bmatrix} I_{4\times4} & 0_{4\times L} \end{bmatrix} \begin{bmatrix} \mathbf{q} \\ \mathbf{x} \end{bmatrix} + \mathbf{v} \tag{12}$$

With these two models, a KF can be applied to estimate the calibration parameters that constitute $\mathbf{x}$. The logic behind the filter that uses these models is as follows. From Eq. (11.a) (which is the first row of Eq. 11.c), when we use the contaminated gyro readings to propagate $\mathbf{q}$ in Eq. (11.c), the propagated quaternion is correct *as long as* $\mathbf{x}$ *is correct*. However, when the estimate of $\mathbf{x}$ is incorrect, the propagated $\mathbf{q}$ is erroneous. The KF compares this $\mathbf{q}$ with the measured quaternion, $\mathbf{q}_m$ and the difference (residual) updates the estimate of $\mathbf{x}$ to bring $\mathbf{q}$ in Eq. (12) to the correct value. Eventually, when the KF compares $\mathbf{q}$ with $\mathbf{q}_m$, we only get the white measurement noise, which means that the filter reaches a steady state and settles on the best estimate of the calibration parameters.

IV. COMPENSATION

To complete the calibration process we need to perform its second stage; namely, compensating the gyro readings with the estimated errors. From Eq. (9.c) we obtain

$$\Delta\hat{\boldsymbol{\omega}} = \begin{bmatrix} \Omega^m & \Omega^k & I_3 \end{bmatrix} \begin{bmatrix} \hat{\mathbf{m}} \\ \hat{\mathbf{k}} \\ \hat{\mathbf{b}} \end{bmatrix} \tag{13}$$

Since

$$\boldsymbol{\omega}_m = \boldsymbol{\omega} + \Delta\boldsymbol{\omega} \tag{14.a}$$

An estimate $\hat{\boldsymbol{\omega}}$ of $\boldsymbol{\omega}$ is computed as follows

$$\hat{\boldsymbol{\omega}} = \boldsymbol{\omega}_m - \Delta\hat{\boldsymbol{\omega}} \tag{14.b}$$

then using Eq. (13) in the last equation yields the final gyro compensation formula

$$\hat{\omega}=\omega_m-\begin{bmatrix}\Omega^m & \Omega^k & I_3\end{bmatrix}\begin{bmatrix}\hat{\mathbf{m}}\\ \hat{\mathbf{k}}\\ \hat{\mathbf{b}}\end{bmatrix} \qquad (15)$$

V. RESULTS

The algorithm was tested using both simulated telemetry and MAP flight data. First, Autonomous Star Tracker (AST) and gyro data were simulated. The AST provides the measured quaternion, $\mathbf{q}_m$. The modeled error values were:

$$\mathbf{m}=\begin{bmatrix}+0.01\\ -0.01\\ +0.01\\ -0.01\\ +0.01\\ -0.01\end{bmatrix} \text{ radians} \qquad \mathbf{k}=\begin{bmatrix}0.01\\ 0.01\\ 0.01\end{bmatrix} \qquad \mathbf{b}=\begin{bmatrix}+0.001745\\ -0.003491\\ +0.005236\end{bmatrix} \text{ rad/sec}$$

Each sensor provided data at a 1 Hz rate. The attitude profile started with an inertial period of 200 seconds, which was used to estimate the gyro biases. This inertial period was followed by three sequential 0.1 deg/sec maneuvers about the x, y, and z-axes, respectively, lasting 200 seconds each. The run length was 1400 seconds. The gyro states were estimated well without performing any tuning on the filter parameters. The resulting gyro calibration *percentage* errors, (true-estimated)*100%, after this simulation were

$$\mathbf{m}_e=\begin{bmatrix}-0.889001\\ 10.360264\\ -1.201588\\ 1.772927\\ -3.215109\\ 8.809881\end{bmatrix} \qquad \mathbf{k}_e=\begin{bmatrix}-2.712136\\ 2.360083\\ -2.330571\end{bmatrix} \qquad \mathbf{b}_e=\begin{bmatrix}0.008048\\ 0.012068\\ -0.000075\end{bmatrix}$$

The time history of the gyro misalignment estimates is shown in Fig. 4. The thick line represents the true value and the thin line represents the estimated value.

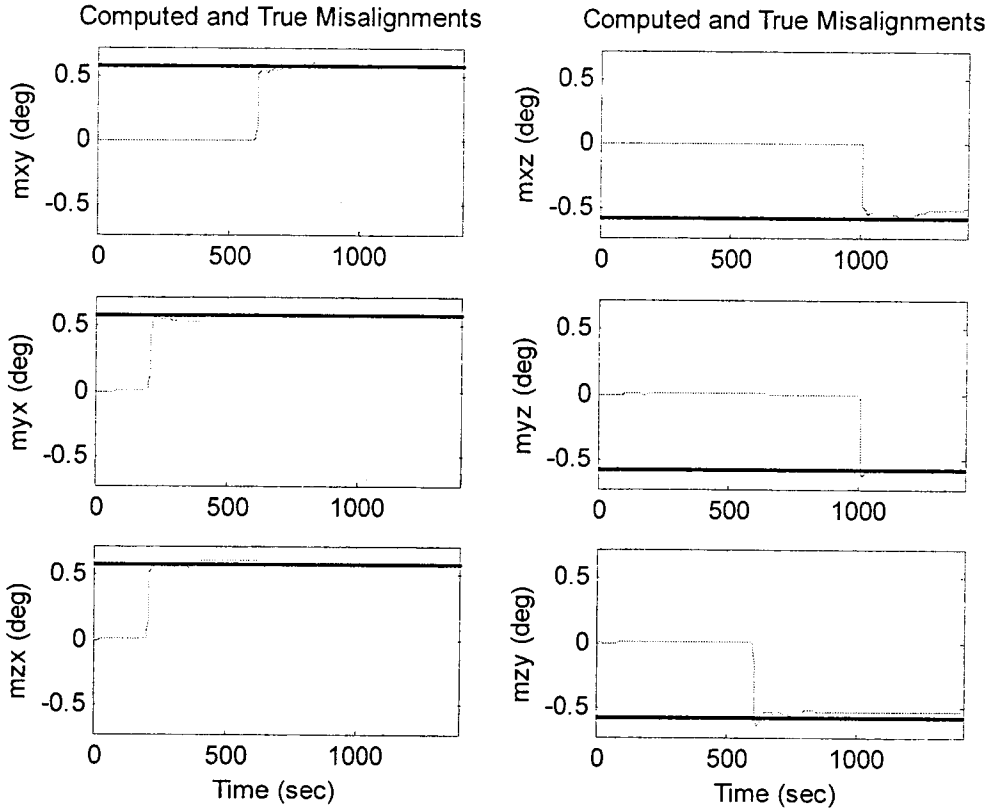

Figure 4: Gyro misalignment estimation versus the true value (the straight line across depicts the true value).

The time history of the gyro scale factors is shown in Fig. 5. Again the thick line represents the true value and the thin line represents the estimated value.

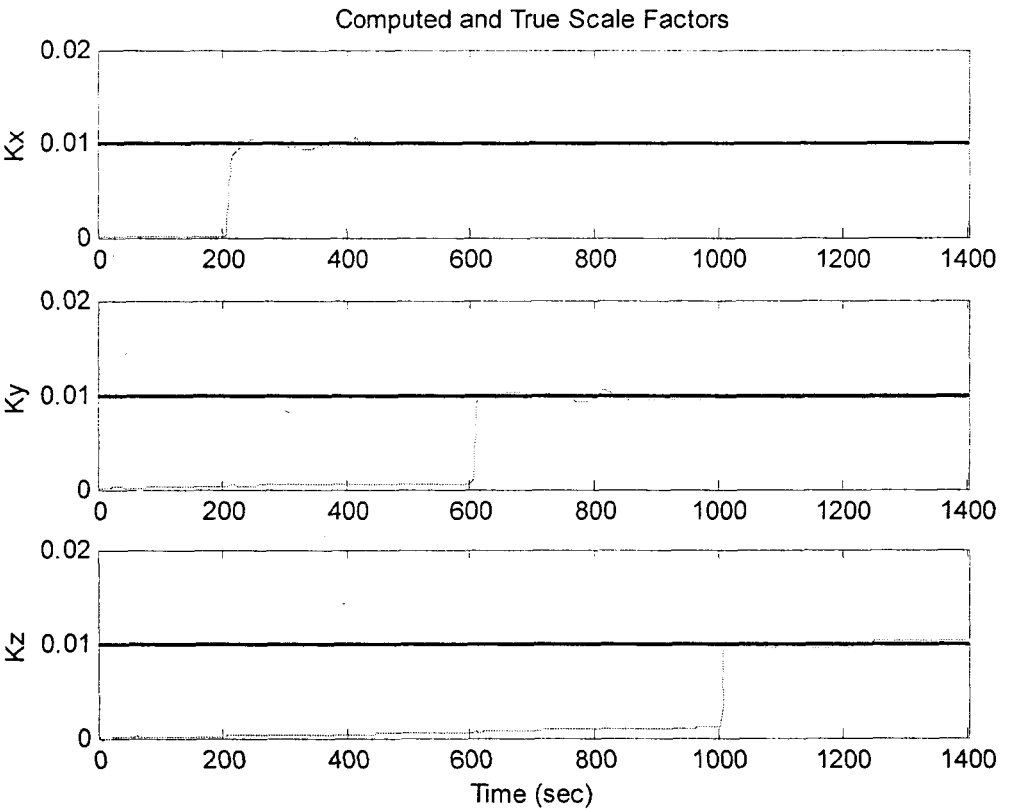

Figure 5: Gyro scale factor estimation versus the true value (the straight line across depicts the true value).

Finally, the time history of the gyro bias estimation is shown in Fig. 6

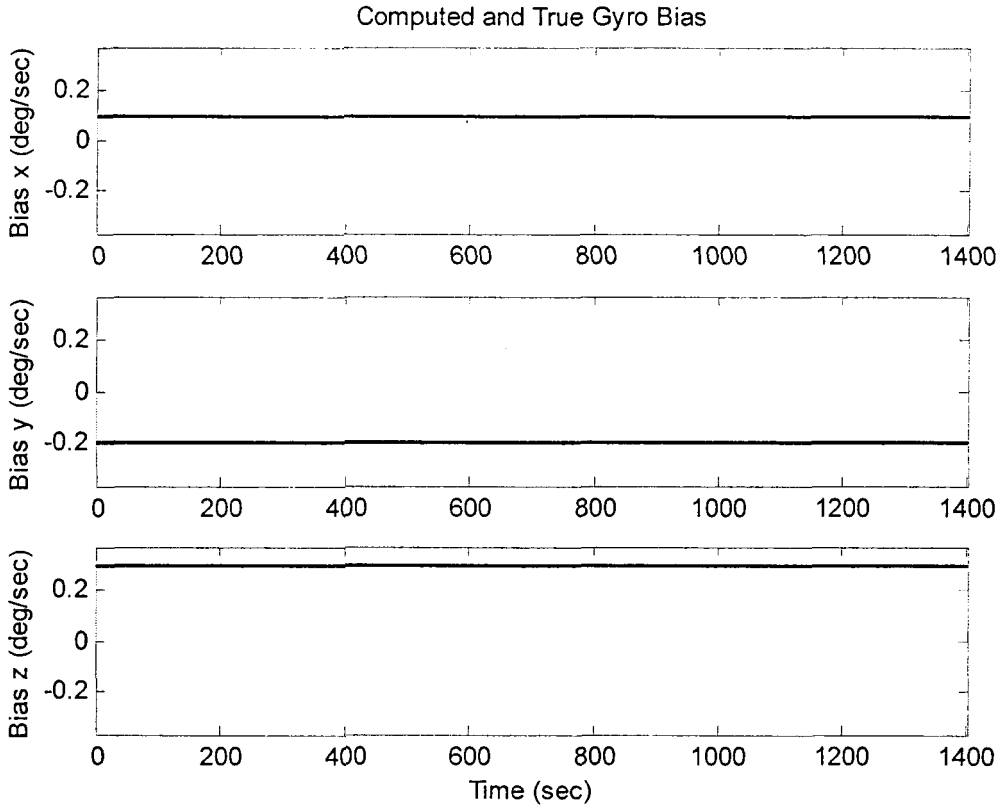

Figure 6: Gyro Bias Estimation versus the true value (the straight line across depicts the true value).

Next, the algorithm was tested using MAP flight data. Shortly after MAP's insertion into the transfer orbit, a series of gyro calibration maneuvers were performed over a 6-hour period using two ASTs and two Digital Sun Sensors (DSSs). The only MAP gyro data readily available for this analysis had already been compensated for the latest calibration parameters. Also, that parameter estimation used all of the above MAP sensors. For this analysis, only one AST and the compensated gyro data was available. For comparison purposes, the single AST and gyro data were processed though the operational system to estimate any residual gyro calibration parameters. Those results were used as the truth model. Those truth parameters are:

$$\mathbf{m} = \begin{bmatrix} 0.001024 \\ 0.000006 \\ -0.000978 \\ -0.000006 \\ -0.000003 \\ -0.000013 \end{bmatrix} \text{ radians} \qquad \mathbf{k} = \begin{bmatrix} 0.000139 \\ -0.004432 \\ 0.000086 \end{bmatrix} \qquad \mathbf{b} = \begin{bmatrix} 0.000000 \\ -0.000000 \\ -0.000000 \end{bmatrix} \text{ radians/sec}$$

As can be seen, the parameters are relatively small. The gyro calibration data consists of 22000 seconds worth of data. The maneuvers consisted of 22 and 44 degree maneuvers each about the x and y spacecraft axes. The final maneuvers of +/- 90 degrees were about the z-axis. The rate history of the maneuvers that were performed for the MAP gyro calibration is shown in Fig. 10. The same compensated gyro data and AST data was input into the gyro calibration algorithm presented here. Using this algorithm the gyro calibration results were:

$$\mathbf{m} = \begin{bmatrix} 0.001176 \\ 0.000002 \\ -0.001061 \\ -0.000002 \\ -0.000001 \\ -0.000002 \end{bmatrix} \text{ radians} \qquad \mathbf{k} = \begin{bmatrix} 0.000000 \\ -0.002681 \\ 0.000000 \end{bmatrix} \qquad \mathbf{b} = \begin{bmatrix} 0.000000 \\ -0.000000 \\ 0.000000 \end{bmatrix} \text{ radians/sec}$$

The misalignment estimation performance is shown in Fig. 7. The scale factor performance is shown in Fig. 8 and the bias estimation performance is shown in Fig. 9. Again, the thick line is the 'truth' and the thin line is the 'estimate'. The performance was excellent overall. However, the *y*-axis scale factor proved to be the most challenging. The boresight of the AST is parallel to the body *y*-axis. Obviously the AST accuracy is least about its boresight, which, in this case, influenced the *y*-axis gyro scale factor estimation.

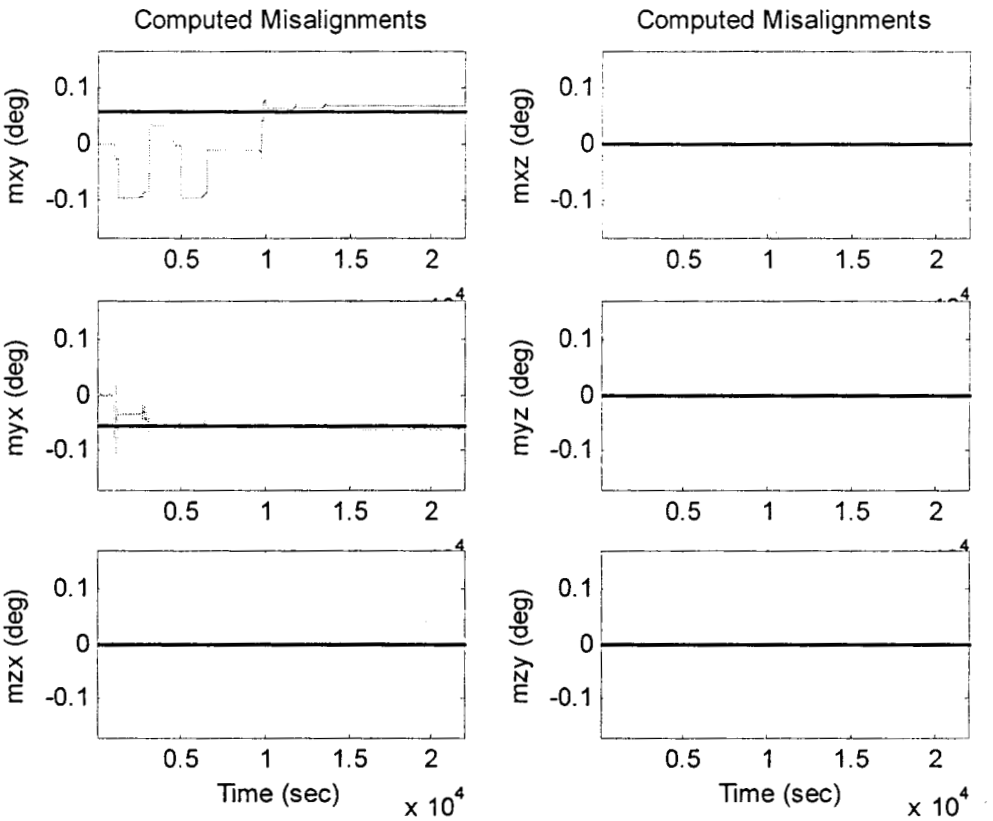

Figure 7: Gyro misalignment estimation versus the true value (the straight line across depicts the true value).

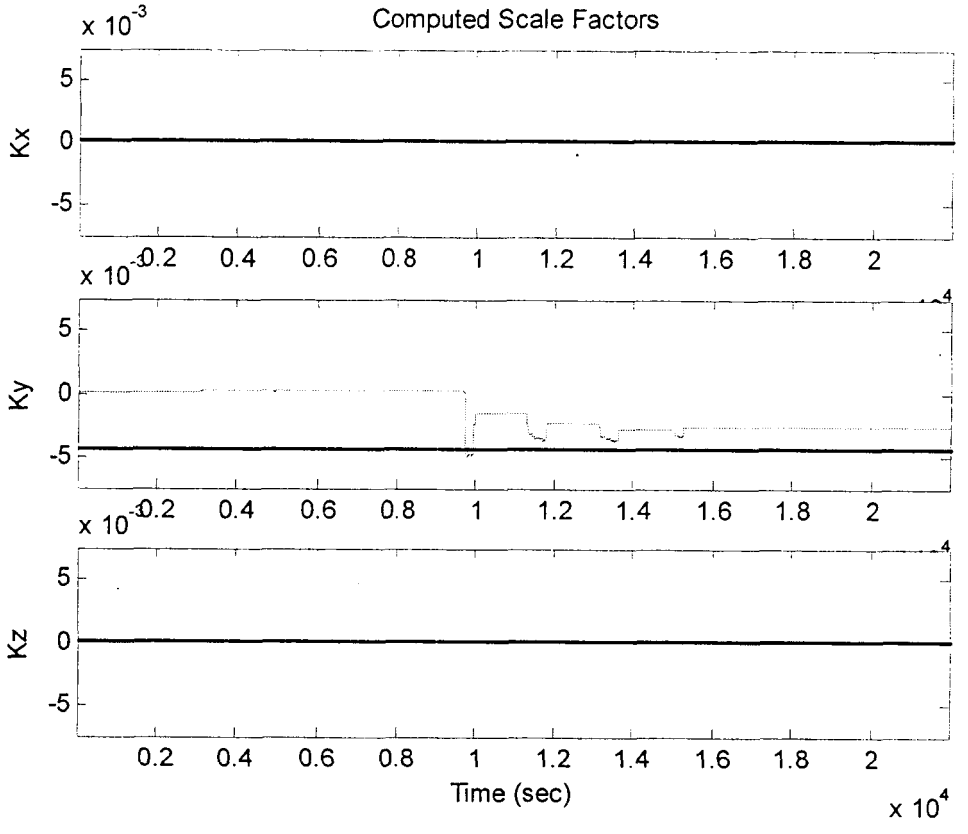

Figure 8: Gyro scale factor estimation versus the true value (the straight line across depicts the true value).

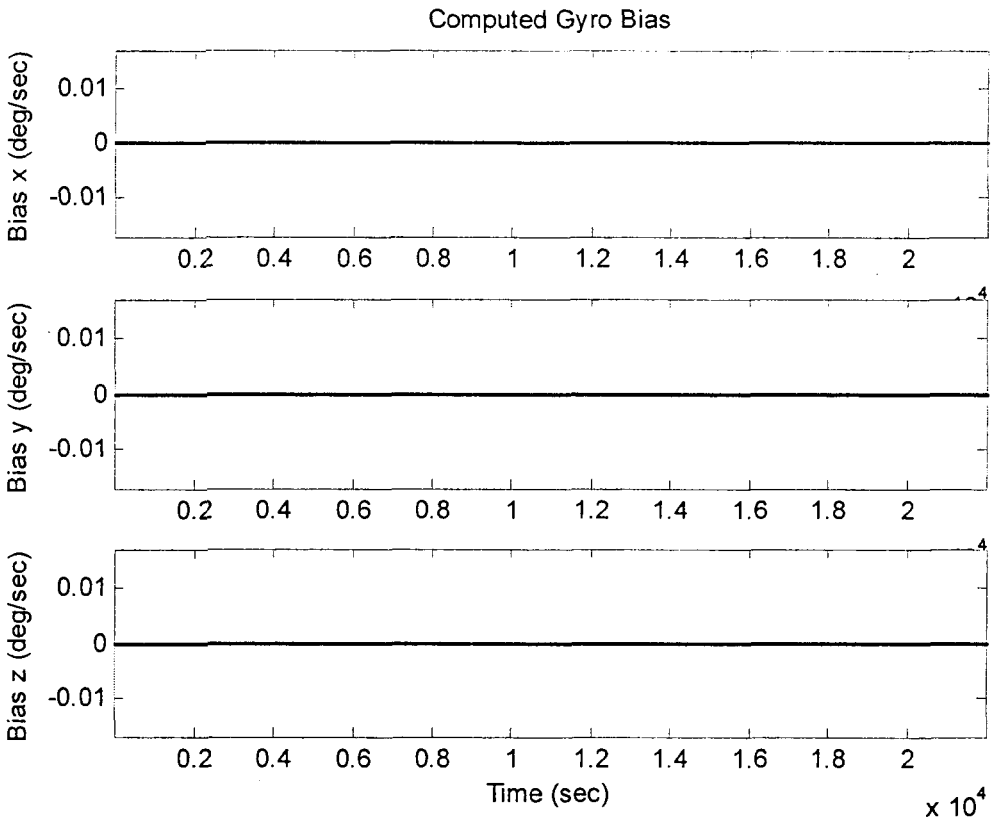

Figure 9: Gyro Bias Estimation versus the true value (the straight line across depicts the true value).

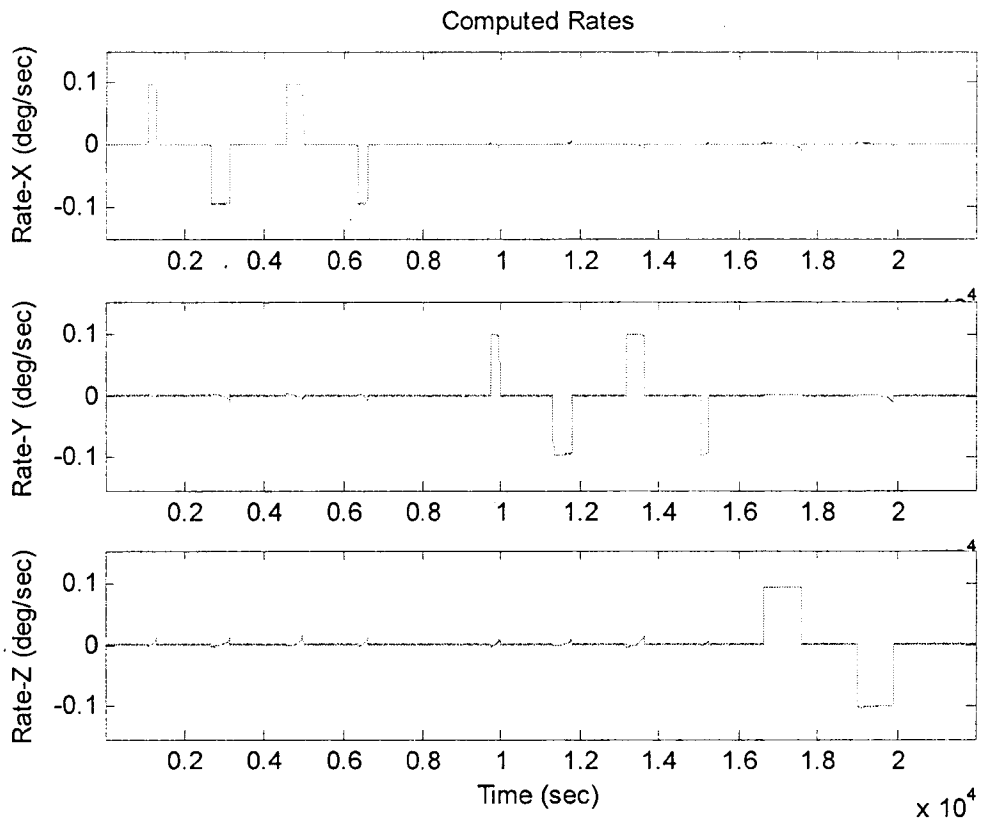

Figure 10: Computed SC rates during the gyro alignment maneuvers.

VII. CONCLUSIONS

In this paper we presented an implicit method of gyro calibration, for the standard orthogonal gyro axes configuration, using a Kalman filter. The filter algorithm used the gyro outputs to supply data for the quaternion kinematics equation. The gyro misalignments, scale factors, and biases were estimated. This method was first tested with simulated data. Upon successful testing with simulated data, the algorithm was tested with MAP flight data. This flight data testing was also successful in estimating the gyro calibration parameters. The size of the errors using the implicit calibration approach was compared to the results presented in the literature for the explicit approach applied to

the AQUA SC. Both approaches provide excellent estimates of the gyro calibration parameters with similar accuracies. However, the implicit approach is less computationally burdensome than the explicit approach, since Euler's equation is not integrated, and actuator data is not required.

Future work will involve testing the algorithm with other spacecraft data and to incorporate vector measurements in addition to the quaternion measurement used in this analysis.

REFERENCES

1 NASA-Goddard Space Flight Center, Multimission Three-Axis Stabilized Spacecraft (MTASS), 553-FDD-93/032R0UD0, 1933, pp. 3.3.2-1 – 3.3.2-10.

[2] Bar-Itzhack, I.Y., and Harman, R.R., "In-Space Calibration of a Skewed Gyro Quadruplet," *AIAA J. of Guidance, Control, and Dynamics*, Vol. 25, No. 5, Sept.-Oct. 2002, pp. 852-859.

[3] Chatfield, A.B., *Fundamentals of High Accuracy Inertial Navigation*, Vol. 174 Progress in Astronautics and Aeronautics, AIAA, 1997, pp. 93-106.